JOURNAL OF GEOPHYSICAL RESEARCH, VOL. ???, NO. , PAGES 1–18,

Diurnal and sub-diurnal effects of the atmosphere on the Earth rotation and geocenter motion

Olivier de Viron[1], Gaëtan Schwarzbaum[1], Francois Lott[2], and Véronique Dehant[1]

O. de Viron, Royal Observatory of Belgium, Brussels, Belgium, o.deviron@oma.be

G. Schwarzbaum, Royal Observatory of Belgium, Brussels, Belgium

F. Lott, Ecole Normale Supérieure, Paris, France, flott@lmd.ens.fr

V. Dehant, Royal Observatory of Belgium, Brussels, Belgium, v.dehant@oma.be

[1]Royal Observatory of Belgium, Brussels, Belgium

[2]Laboratoire de Météorologie Dynamique, Ecole Normale Supérieure, Paris, France.

Abstract. The diurnal cycle in the atmospheric angular momentum (AAM) and in the wind and surface pressure fields is studied with a realistic Atmospheric General Circulation Model (GCM) in which the AAM budget is very well closed. For this, we used a one year simulation. From a geodetic point of view, we find that this model predicts AAM variations at diurnal timescale which produce a polar motion near 0.2 milliarcsecond. Additionally, at the same period, the model predicts a geocenter motion of the order of the millimeter. These results are compared with those obtained with the NCEP/NCAR and ECMWF operational analysis data sets. As the AAM budget is not exactly closed in those two datasets, large quantitative differences with the GCM are found. These results witness that there are problems in using AAM values from the major weather prediction center to estimate the AAM and torques variation at diurnal and subdiurnal timescales. We have also computed, for the three models, the spherical harmonics decomposition of the diurnal and semi-diurnal surface pressure signals. The results show large differences from one model to another, which advices carefulness when correcting gravity missions (as GRACE for instance) from the high frequency effect of the atmosphere on the orbit, using operational analysis.

1. Introduction

The interaction between the Earth and its superficial layers (atmosphere, ocean and hydrology) is a major cause of changes in the Earth rotation for period ranging between several hours and several years. In particular, and if we exclude the well predicted oceanic tides, the atmosphere is known to dominate the Earth rotation variations between several hours and several years (see for instance *Barnes et al.* [1983]).

The Earth rotation fluctuations can be decomposed into three different components: the variations of the rotation speed, associated with changes in the length-of-day (LOD), the motion of the solid Earth around its rotation axis, known as the polar motion, and the motion of the Earth rotation axis in space, known as precession-nutation. The effect of the atmosphere on Earth rotation can be studied by two different and complementary, methods: (1) the angular momentum approach, in which the Earth-Atmosphere system is considered as isolated, and the Earth rotation variations are computed from the change in the atmospheric angular momentum (AAM); and (2) the torque approach, for which the interaction between the solid Earth and the atmosphere is evaluated directly (See *Wahr* [1982] for more details about the two approaches). The two approaches are linked by the angular momentum budget equation of the atmosphere: the rate of change of the AAM is equal to the total torque acting on the atmosphere at the Earth/ocean surface.

Each of the three components of the AAM is composed of two parts: a mass term (or pressure term) associated with a rigid rotation of the atmosphere with the Earth, and a wind term (or motion term) associated with the relative motion of the atmosphere with respect to the Earth. The total torque is composed of an ellipsoid contribution (resulting from the pressure force and gravitational interaction between the Earth bulge and the

atmosphere), a mountain torque related to the pressure acting on the topography, and a friction torque (See *Wahr* [1982]). In GCMs, this latter torque is computed from the surface stress predicted by the model boundary layer turbulence parametrization. Additionally, the mountain torque is complemented by a torque related to surface stress due to the subgrid scale orography parametrization (*Lott and Miller* [1997], for the ECMWF model and for the LMD GCM).

In this paper, we focus on the AAM changes in the diurnal band, which are very important for the nutation of the Earth. Indeed, the conservation of the Earth-Atmosphere angular momentum impose that the atmospheric motion at quasi-diurnal retrograde period is compensated by nutational motion of the solid Earth. This effect has been evaluated using the angular momentum approach, for instance by *Bizouard et al.* [1998], and using the torque approach by *Dehant et al.* [1996]. This last study has shown that the atmospheric effect on nutation, when evaluated using the torque approach, was too large by at least one order of magnitude with respect to the observed nutation of the Earth. This problem has been studied in *de Viron et al.* [2001] and *Marcus et al.* [2004]. They used data from the NCEP/NCAR (National Center for Environmental Research/National Center for Atmospheric Research) reanalysis model (*Kalnay et al.* [1996]) and show that the problem was in the torque approach, and comes from an ill-conditioned problem: the angular momentum budget has to be considered in an inertial frame, and in this frame the AAM variations are slow (diurnal retrograde in the rotating frame becomes low frequency in the inertial frame), which implies a small torque. As this small torque should result from a nearly exact cancellation between a large ellipsoidal torque (global effect of the atmospheric mass acting on the Earth bulge) and the local torques due to mountains and

boundary layer stresses, it can only be obtained if the torques can be estimated with a very good precision, which could not be achieved with the NCEP/NCAR reanalysis data (*de Viron et al.* [2001] and *Marcus et al.* [2004]).

In this paper, we used a one year simulation with the LMD atmospheric GCM (see for instance *Lott* [1999]). The evolution of this GCM is never interrupted by any assimilation procedure (unlike the ECMWF and the NCEP models), which ensures a very good closure of the angular momentum budget. In this model, we analyzed the three components of the AAM budget, and deduce the predicted torques at diurnal and subdiurnal periodicities. In addition, we evaluate the effect on the Earth rotation and geocenter motion. We also compare the atmospheric forcing, for the frequencies allowed by each model sampling, to those computed from the output of the NCEP reanalysis and from the ECMWF (European Center for Medium-range Weather Forecast) reanalysis.

The plan of the paper is as follows. Section 2 presents the different datasets used. Section 3 compares the diurnal cycles in flow field from the 3 datasets, focusing on those which matter for AAM and torques, that is the surface pressure and the barotropic wind. After this evaluation of the model performance, Section 4 analyzes the AAM budget and some consequences on the Earth rotation parameters. Section 5 concludes and discusses the significance of the results in Section 3 to the dealiazing of gravity missions, such as GRACE and CHAMPS from the diurnal tides in the surface pressure. It also discusses the significance of the results in Section 4 to the prediction of the diurnal variations of the EOP from the major prediction center operational analyses.

2. Simulation and model used

The LMD-GCM we use is a gridpoint model, with a 2.5^ox2.5^o horizontal resolution and 19 vertical levels, most of them spanning the entire troposphere but a few of them are in the stratosphere. It is forced by climatological sea surface temperature and sea ice cover, a configuration for which its climatology is realistic (*Lott* [1999]). In time, this model solves all adiabatic processes (advection + pressure forces) explicitly, yielding a short temporal resolution (dt=30s). In this context, the adiabatic processes (radiation, boundary layer and subgrid scale orography parametrizations) are called every 15 min only.

In the present paper, we use a 1 year simulation of the LMD-GCM, and evaluate every hour the barotropic wind and the various surface stresses associated with the physical parameterizations and the surface pressure. From these 2D fields, we evaluate the AAM budget and verifies that, for the three components, it is very well closed.

We also extract the same fields from the ECMWF operational analysis every three hours for the calendar years 2002 and 2003, and for the NCEP reanalysis every six hours for the same calendar years. Note that in those two data sets, the surface stresses are produced by short-range forecast, yielding in part to the inconsistencies between the AAM approach and the torque approach noted in the introduction.

From these different sets of data, we extract a "mean day", computed by averaging the value at each given hour of the output on an integer number of years: 2 years for NCEP and ECMWF (2002-2003), and one "climatological year" for the LMD.

At these frequency, we do not use the inverted-barometer approximation to correct geodetic forcing for a static ocean response, as it is accepted to be only valid at periods

for which the ocean has time to readjust, i.e. periods longer than a few days (see *Munk and McDonald* [1960]).

The axe system is defined as follow: the Z axis is along the Earth mean rotation axis, the X axis is in the mean equatorial plan, and pointing to the Greenwich meridian, and the Y axis is at 90 degrees from the X axis in the mean equatorial plane. In this system, the LOD variation are associated with AAM variations and torques in the Z component and the polar motion and nutation with the X and Y components of AAM and torques.

3. The diurnal cycle in pressure and barotropic wind and its sub-harmonics

The atmospheric mass distribution affects the angular momentum, which is estimated from the surface pressure field. The motion term is estimated from the barotropic wind. In this section, we discuss the pattern of the S_1 and S_2 waves in the pressure and barotropic wind fields.

In Figure 1, we show the variation, for the mean day, of the surface pressure average over the latitude (with a $\cos\phi$ weighting). The amplitude and phase of the three models are fairly close, considering the different time resolutions of the models. Note that the NCEP, with 6 hourly data, is unable to catch the regular westward propagation of the wave, and simply show a standing wave with 6 hourly period. The Movie 1 shows the same evolution for the three models on the mean day, in 2 dimensions.

Figure 1

Movie 1

It is known for a long time that the dominant signal in the high frequency band of the surface pressure is linked to the resonant S_2 waves (see for instance *Chapman and Lindzen* [1970]). This wave was first estimated from ground measurement and, more recently, *Ponte and Ray* [2002] have estimated it by an interpolation of the ECMWF data, using a method proposed by *Van den Dool et al.* [1997].

The S_1 wave is very different in nature, as it is not a resonant mode of the atmosphere, but barely a local response of the atmosphere to daily cycle of continental surface temperature, the sea surface temperature not reacting much to the daily cycle in insolation. According to these two factors, there is no propagation of the S_1 pressure wave, but rather a standing wave over the continent, as it can be observed on the Movie 2. **Movie 2**

In order to be associated with AAM matter term variations, the pressure field has to present particular geographical patterns: the Earth rotation speed is affected only if the inertia of the atmosphere along the mean rotation axis changes, which, in terms of spherical harmonics, is a degree 2 order zero. The polar motion will only be affected by distribution of degree 2 order 1, and the geocenter motion by degree 1 order 0 the Z axis, and by degree 1 order 1 for the X and Y axes.

To allow a thorough comparison, Table 1, Table 2, and Table 3 give the spherical harmonic decomposition of the surface pressure for the waves S_1, S_2, S_3, and S_4 for the ECMWF and LMD model. In those Tables, we go up to degree 10, to allow comparison with the coefficients used in the dialiasing of the spatial gravity missions as GRACE or CHAMP. The coefficients are quite similar for the S_1 waves from the NCEP reanalysis and LMD model, and the values from the ECMWF analysis present phase differences at the level of some tens of degree. **Table 1** **Table 2** **Table 3**

As well known from *Chapman and Lindzen* [1970], for instance, the S_2 wave is dominated by a degree 2 order 2 wave, and S_1 by a degree 1 order 1 wave. In Table 1 and 2, note that this part of the signal is fairly consistent from one model to another. The part of the signal relevant for Earth rotation (degree 2 order 0 and 1) is quite smaller, and

differs to a large extend from one model to the other, which implies a tiny (and not very reliable) effect on the Earth rotation.

The barotropic wind (i.e. the wind integrated vertically over the pressure column), shown in Figure 2, present similarities between S_1 and S_2: it is dominated by a convergence-divergence field at global scale, but with two convergence points (and 2 divergence points) for S_2 and only one for S_1. Additionally, the size of the S_2 wind signal does not reflect the ocean-continent distribution, as it is the case for the S_1 wave.

Figure 2

Again, this wind distribution is inefficient to generate a variation in Earth rotation: the motion term of the angular momentum is associated with the mean rotation of the atmosphere, which correspond to the rotational part of the wind field. A purely divergent field has no rotation part, so the wind term is small as well. It will be smaller for the S_2 wave than for the S_1 wave, because the ocean-continent distribution perturbs the purely divergent field for S_1 and not for S_2.

Consequently, using only the pattern in the pressure and wind field, we can expect the effect on Earth rotation to be small, and even smaller for S_2 than for S_1 and not very consistent from one model to another. We can also expect a larger and more consistent effect on the equatorial geocenter motion. Even if there is a large diurnal and semi-diurnal signal in the atmosphere, the effect on the Earth rotation is expected to be small.

4. Diurnal angular momentum budget of the atmosphere and Earth rotation

4.1. AAM Budget in the LMD-GCM

The angular momentum budget equation is given by

$$\frac{d\vec{H}_{\rm mass}}{dt} + \frac{d\vec{H}_{\rm wind}}{dt} + \vec{\Omega} \wedge \left(\vec{H}_{\rm mass} + \vec{H}_{\rm wind}\right) = \vec{\Gamma}_{\rm Ellips.} + \vec{\Gamma}_{\rm Mount.} + \vec{\Gamma}_{\rm Fric.} + \vec{\Gamma}_{\rm Grav.W} \quad (1)$$

where the time derivative are computed in the Earth fixed reference frame and $\vec{\Omega}$ is the Earth rotation vector. The expression for computing the different torques and the angular terms has been published in several studies, as *Barnes et al.* [1983], *Wahr* [1982] and *de Viron et al.* [2001], and we will not repeat them here.

Figure 3 shows the AAM time derivative and the total torque for the "mean day" from the three models. It can be observed that the angular momentum budget equations are well closed in the LMD model and not in the reanalysis. Note also that both the AAM time derivatives and the torques differ strongly from one dataset to the other. Consequently, in this study, we will next focus on the GCM LMDz results only. It does not mean that the results are closer to reality, but we can only investigate the angular momentum budget if it is reasonably well closed. Note nevertheless that as our model has realistic tides (see Section 3), we can nevertheless expect that the results from the GCM LMDz will be relevant for the real atmosphere.

Figure 3

Figure 4 shows the angular momentum budget for S_1, S_2, and S_3 from the LMD model, for the three components, and using a phase plot representation (the X component is the AAM budget closure in phase with the civil time, and the Y component is the AAM budget in quadrature). This representation allows to visualize directly the relative amplitude of the different terms in this budget, and to discuss their relative importance. The first observation that can be done is that the contribution from the mass term and wind term tends to cancel each other, for the three components and for the three waves. It means again that we need a good precision in order to compare the AAM terms, the total AAM being a residual between two large contributors.

Figure 4

For the X component, the ellipsoidal torque dominates, but not as strongly as at synoptic timescale, for which the mountain torque is very small (see *de Viron et al.* [1999]). For the Y component, S_1 produce a large ellipsoidal torque, most of it being cancelled by the other torques.

As, for the diurnal torque, the dynamics at regional scale is very important (mostly for the mountain torque), it is important to localize where the interaction occurs, which is possible by integrating on every continent and ocean separately. As explain in previous studies (for instance *de Viron et al.* [2001]), the mountain torque results from the product of the surface pressure by the topography derivative, only the longitude derivative being relevant for the Z component, and both longitude and latitude derivative for the equatorial components. In that paper, Antarctica was said to be dominant for the equatorial component, in the time domain. Of course, this is not expected to be the case for the diurnal cycle, as those high latitude only present a small, if any, diurnal cycle in the surface pressure. In our study, we find the Asia (Himalaya) to be, by far, the major contributor for the equatorial exchange of angular momentum, with some effect, mostly in the Y component, of the South America. For the axial torque, the Asia and South America dominates the exchange, which is not surprising considering the longitude derivative of the topography, as shown in Figure 1 of *de Viron et al.* [2001], for instance. The major contributions from the friction torque occur over the same continents: Asia and South America. The same is also true for the gravity-wave drag torque, with an additional noticeable contribution from Africa in the diurnal torque.

4.2. Equatorial AAM budget at diurnal period

When studying the effect on Earth rotation, it makes sense to look at the budget in terms of prograde and retrograde waves. The prograde diurnal in the Earth reference frame will be associated with high frequency polar motion, and the retrograde diurnal will be associated with nutation. Mathematically, it is equivalent to decompose an elliptic motion (periodic motion of different amplitude in X and Y) into two circular motions, one in the same direction as the Earth rotation and one in the opposite direction. The mathematical expression to use are given for instance in *Dehant et al.* [1996]. Figure 5 shows the AAM budget for the equatorial components, decomposed in prograde and retrograde terms. Again, the angular momentum budget is fairly well closed, with the retrograde wind term much larger than the equivalent matter term. This last results is consistent with other studies (see *Bizouard et al.* [1998], for instance). In Figure 5, note as well that the ellipsoidal torque is near exactly cancelled by the other torques. This confirms the hypothesis made by *de Viron et al.* [2001] and *Marcus et al.* [2004] that such a balance was the necessary condition to close the AAM budget in the retrograde diurnal frequency band. Nevertheless, note that, in the model, the friction torque contribution is substantially smaller than the mountain torque, which was not the case in the NCEP reanalysis in *de Viron et al.* [2001] and *Marcus et al.* [2004]. The prograde component does not have the same dynamic constraint as the retrograde, and the ellipsoidal torque dominates strongly the others as shown on Figure 5.

Figure 5

4.3. Impact on the Earth Orientation Parameters

In the LMD-GCM, the torque and the angular momentum approach are equivalent, as the angular momentum budget equation is verified. Consequently, we will use the

angular momentum approach to evaluate the Earth rotation effect. Table 4 gives the Earth rotation effect, for the S_1, S_2, and S_3 waves (when meaningful) for the three models. As expected from the results in Section 4, the amplitude and phase of the effect, according to the different models, are very different. For the S_1 wave, there is a reasonable agreement in amplitude and phase between the results from the NCEP model and from the LMD model. The ECMWF results differ both in amplitude (nearly a factor 5) and in phase. This difference between the ECMWF results and the LMD results also appear for the higher frequencies. At the S_1 frequency, the size of the polar motion is at the level of 0.2 mas (according to the LMD and NCEP model) or 1 mas (according to the ECMWF). Without additional information, it is difficult to determine which among these datasets gives the right answer, if any.

Table 4

4.4. Diurnal and sub-diurnal geocenter displacement

The position of the geometrical center of the terrestrial reference frame, i.e. position of the crust, with respect to the center of mass of the Earth is given by:

$$\begin{aligned} x_{CM} &= \frac{a^3}{M_T}\left(1+\frac{M_L}{M_T}\frac{h_1+2l_1}{3}\right)\int_S \Delta\sigma \sin^2\theta\cos\lambda \; d\theta d\lambda, \\ y_{CM} &= \frac{a^3}{M_T}\left(1+\frac{M_L}{M_T}\frac{h_1+2l_1}{3}\right)\int_S \Delta\sigma \sin^2\theta\sin\lambda \; d\theta d\lambda, \\ z_{CM} &= \frac{a^3}{M_T}\left(1+\frac{M_L}{M_T}\frac{h_1+2l_1}{3}\right)\int_S \Delta\sigma \sin\theta\cos\theta \; d\theta d\lambda, \end{aligned} \tag{2}$$

where a is the Earth mean radius, M_T is the mass of the Earth, M_L is the total mass of the load, h_1 and l_1 are the load Love number, as defined by *Farrell* [1972], and $\Delta\sigma$ is the atmospheric mass distribution corresponding to the tidal wave. Table 5 gives the geocenter motion, for the S_1, S_2, and S_3 waves (when meaningful) for the three models.

Table 5

As shown in Section 3, the diurnal pressure waves have a strong degree one, order one spherical harmonic component, which is associated with a geocenter displacement in the equatorial plan.

Note that, unlike for the Earth rotation, the diurnal geocenter signal is very similar from one model to the other. This signal is large, which is not surprising when considering the diurnal part of Figure 1, where the degree one pattern of the surface pressure distribution is very clear. This consistency between the models gives us much more confidence for the diurnal geocenter motion than for any of the other quantities we estimate here.

5. Conclusion

In this study, we used three different atmospheric datasets to analyze the geodetic consequences of the diurnal and semi-diurnal atmospheric tides. We show that the three models differ strongly. Consequently, it is difficult to consider our results as more than orders of magnitude. Nevertheless, our analysis provides important qualitative insights on atmospheric effects on geodetic parameters at diurnal and subdiurnal timescale.

First, we estimated the spherical harmonic decomposition of the surface pressure, and found differences between the LMD model and the NCEP reanalysis, on the one hand, and between the LMD model and the ECMWF analysis on the other hand. As this last model is used to de-aliase the GRACE data from the high frequency signal, we advise caution for the semi-diurnal cycle.

We also used the LMD model (purely dynamical model, with no data assimilation) to study the angular momentum budget of the atmosphere at diurnal time scales. We confirm the assertion of *de Viron et al.* [2001], that the budget is closed in the diurnal

retrograde band because the ellipsoidal torque is nearly exactly compensated by the local torque (here, mostly the mountain torque).

We then investigate the effect on some geodetic observable, namely the Earth rotation variation (LOD variation and polar motion) and the geocenter motion. We show that the three models predict very different Earth rotation variation, both for diurnal and semi-diurnal period. On the contrary, they predict quite similar geocenter motion at diurnal period. This difference comes from geometrical reason: the diurnal and semi-diurnal signal in the pressure and the wind are rather inefficient to create AAM variation. Consequently, the AAM changes comes from the very small part of the wind and pressure field which has the right pattern. The opposite occurs for the diurnal geocenter motion: the S_1 pressure wave has the right geometry to generate geocenter motion; consequently, the dominant part of the signal (which is common from one model to another) is directly efficient. This results in a large and consistant geocenter motion. Even if S_2 is the larger signal in the sub-diurnal band, its spherical harmonic of degree 2 and order 2 geometry prevents it to generate noticeable effects on the Earth orientation parameters or geocenter location. Indeed the LOD is affected by atmospheric patterns that are zonally symmetric, the polar motion and the geocenter motion by patterns of zonal wave number 1, and the S_2 wave is dominated by a zonal wave number 2 structure. On the contrary, the S_1 waves has a signal large enough to create observable signal on polar motion (at the level of 0.2 mas), and geocenter (1 mm). This last result is the more robust, as the datasets agree to a certain extent on the evaluation.

Acknowledgments. The work of OdV was financially supported by the Belgian Service Public fédéral de Programmation Politique scientifique.

References

Barnes R. T. H., Hide R., White A. A. and Wilson C. A., Atmospheric angular momentum fluctuations, length-of-day changes and polar motion, *Proc. R. Soc. London*, A 387, 31-73, 1983.

Bizouard C., Brzezinski, and Petrov S., Diurnal atmospheric forcing and temporal variations of the nutation amplitudes, J. Geodesy, 72, 561-577, 1998.

Chapman S., R.S. Lindzen, Atmospheric Tides, Thermal and Gravitational, D. Reidel Publishing Company, Dordrecht-Holland, 200p, 1970.

Dehant, V., C. Bizouard, J. Hinderer, H. Legros, and M. Lefftz, On atmospheric pressure perturbations on precession and nutations, *Phys. Earth Planet. Inter.,* 96, 25-39, 1996.

de Viron, O., C. Bizouard, D. Salstein, and V. Dehant (1999), Atmospheric torque on the Earth and comparison with atmospheric angular momentum variations, J. Geophys. Res., 104(B3), 48614876.

de Viron O., S.L. Marcus, and J.O. Dickey, Diurnal angular momentum budget of the atmosphere and its consequences for Earth's nutation, *J. Geophys. Res.,* B11,26,747-26,759, 2001.

Farrell, W. E., Deformation of the Earth by surface load, *Rev. Geophys. Space Phys.*, *10*, 761-797, 1972.

Kalnay, E., M. Kanamitsu, R. Kistler, W. Collins, D. Deaven, L. Gandin, M. Iredell, S. Saha, G. White, J. Woollen, Y. Zhu, A. Leetma, R. Reynolds, M. Chelliah, W. Ebisuzaki, W.Higgins, J. Janowiak, K. C. Mo, C. Ropelewski, J. Wang, R. Jenne amd D. Joseph, The NCEP/NCAR 40-Year Reanalysis Project, *Bull. Amer. Meteorol. Soc.*, *77*, 437–471, 1996.

Lott, F., 1999, Alleviation of stationary biases in a GCM through a mountain drag parametrization scheme and a simple representation of mountain lift forces, *Monthly Weather Review*, **127**, 788–801.

Lott, F., and M. Miller, 1997, A new subgrid scale orographic drag parameterization; its testing in the ECMWF model, *Quarterly Journal of the Royal Meteorological Society*, **123**, 101–127.

Marcus S.L., O. de Viron O., and J.O. Dickey , Atmospheric Contributions to Earth Nutation: Geodetic Constraints and Limitations of the Torque Approach, *J. Atm. Sci*, 61 (3), 352-365, 2004.

Munk, W.H. and McDonald, G.F., The Rotation of the Earth, a Geophysical discussion, Cambridge University Press, 323pp., 1960.

Ponte, R. M., and R. D. Ray (2002), Atmospheric pressure corrections in geodesy and oceanography: A strategy for handling air tides, Geophys. Res. Lett., 29(24), 2153, doi:10.1029/2002GL016340.

Van den Dool, H. M., S. Saha, J. Schemm, and J. Huang, A temporal interpolation method to obtain hourly atmospheric surface pressure tides in Reanalysis 1979 1995, J. Geophys. Res., 102, 22,013 22,024, 1997.

Wahr, J.M., The effects of the atmosphere and oceans on the Earth's wobble, 1, Theory, *Geophys. J. R. Astron. Soc*, *70 (2)*, 329-372, 1982.

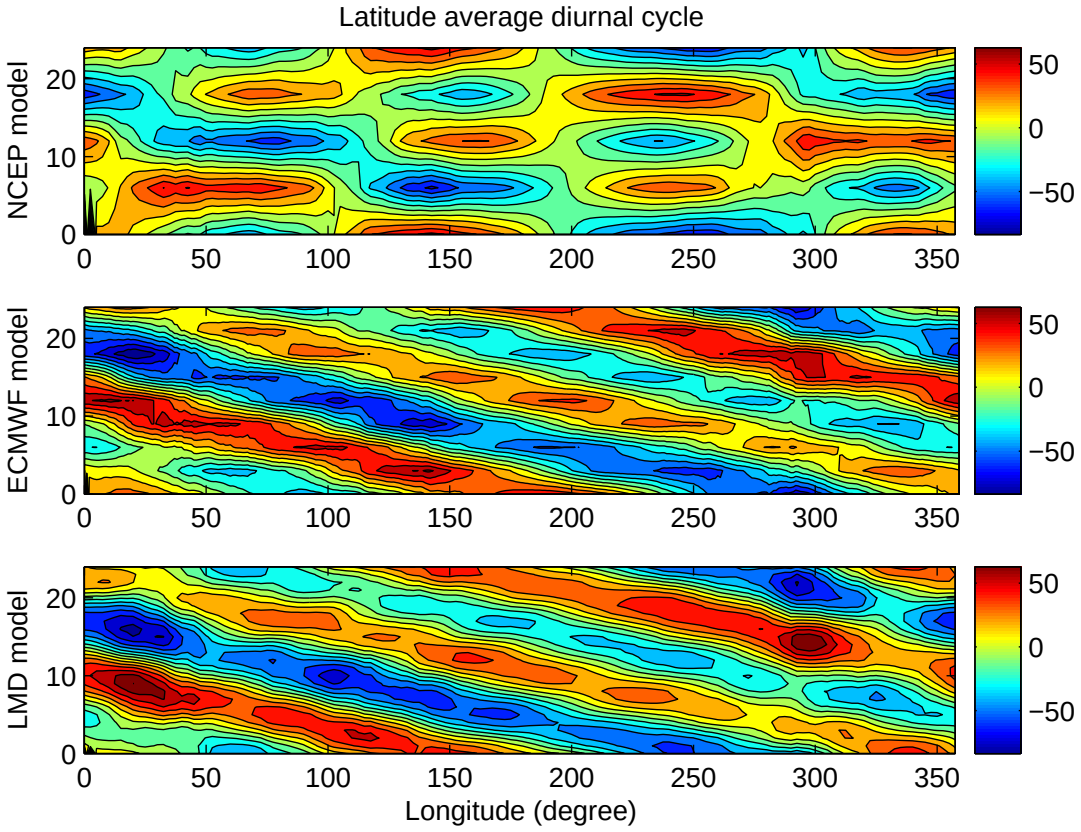

Figure 1. Latitude averaged pressure variation for the three models. The y axis in the figure is the time of the day, in hour.

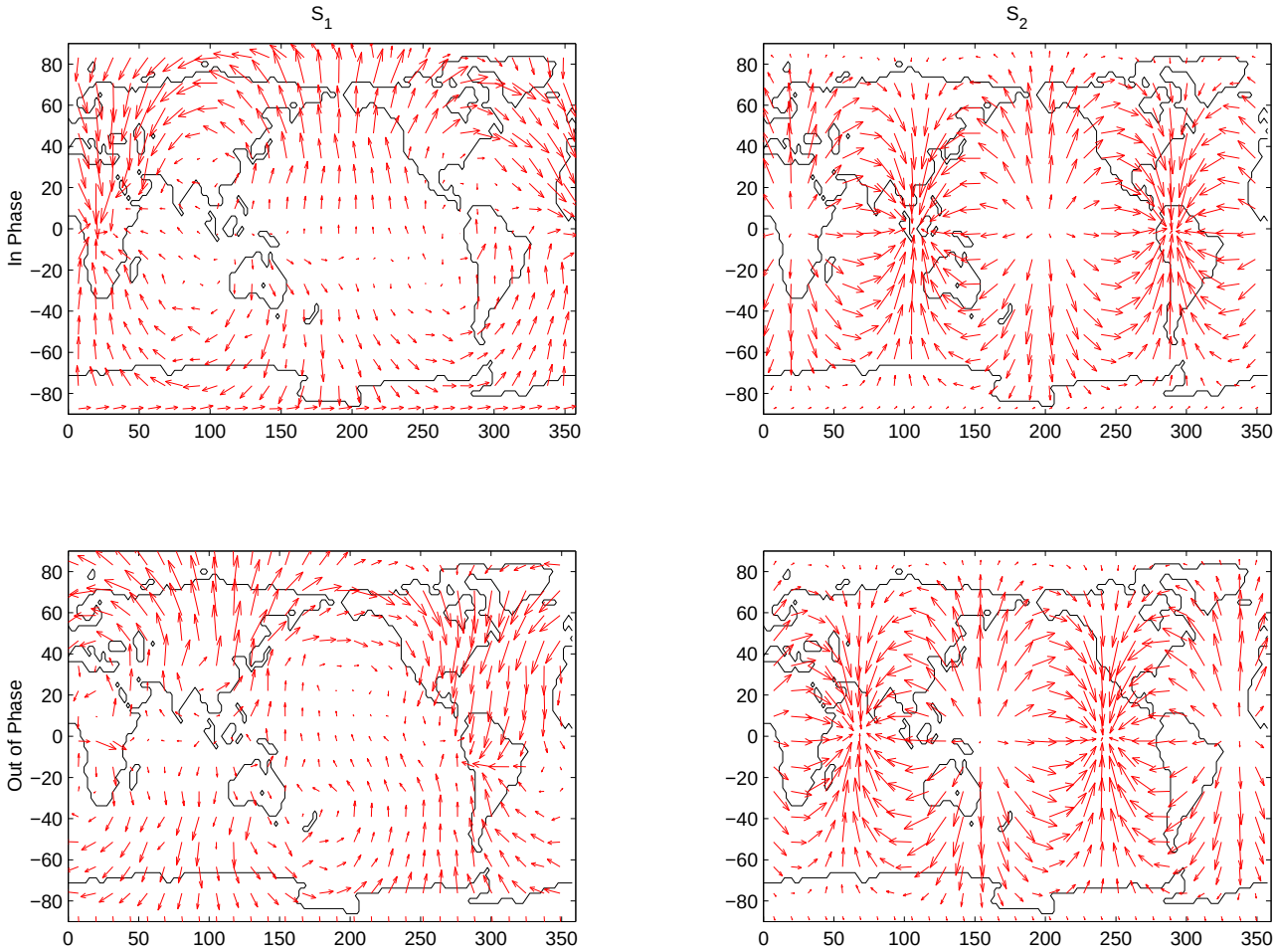

Figure 2. The barotropic wind for S_1 and S_2 in the LMD model.

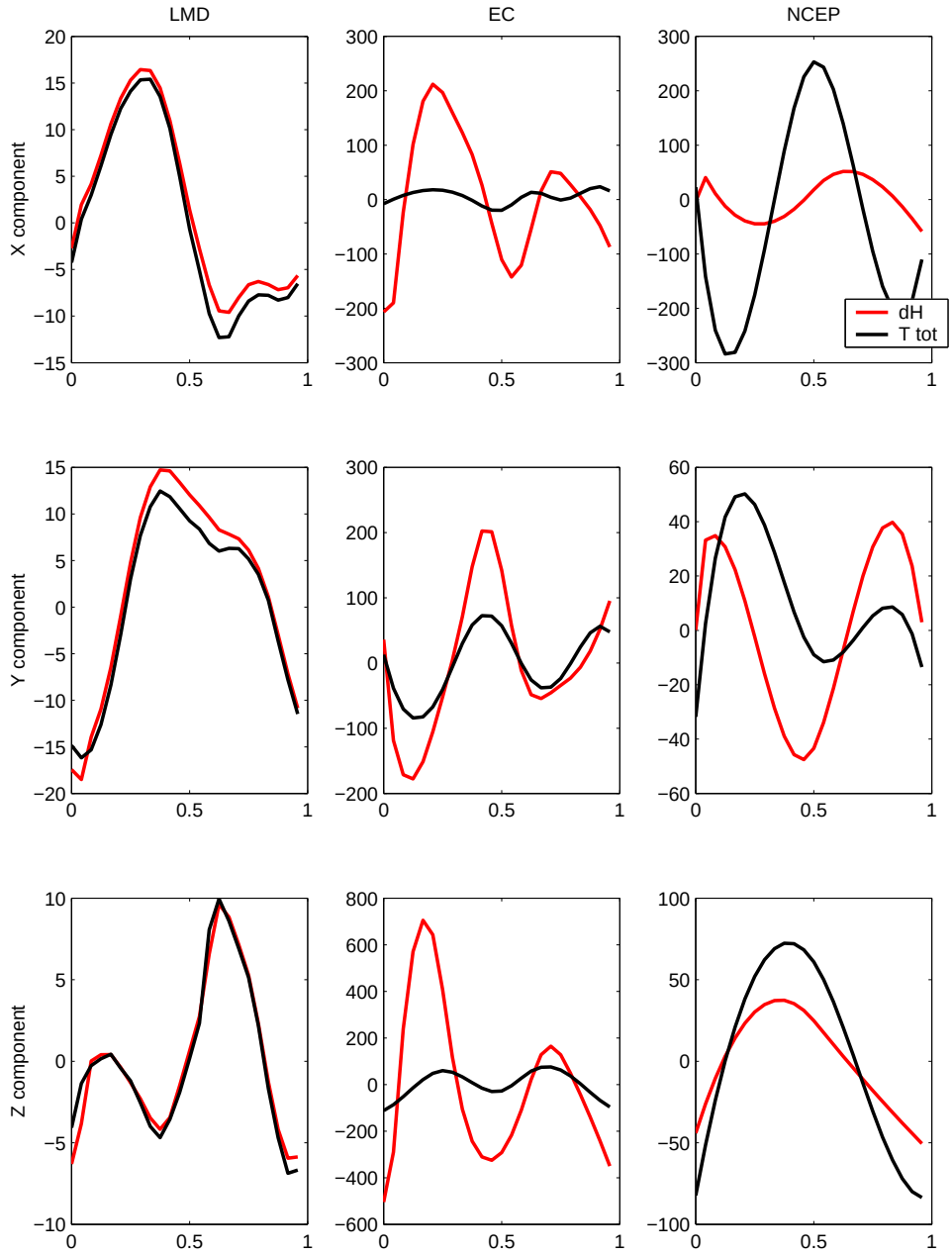

Figure 3. Angular momentum budget equation for the three models (unit=Hadleys).

The NCEP and EC results have been interpolated using their harmonics development.

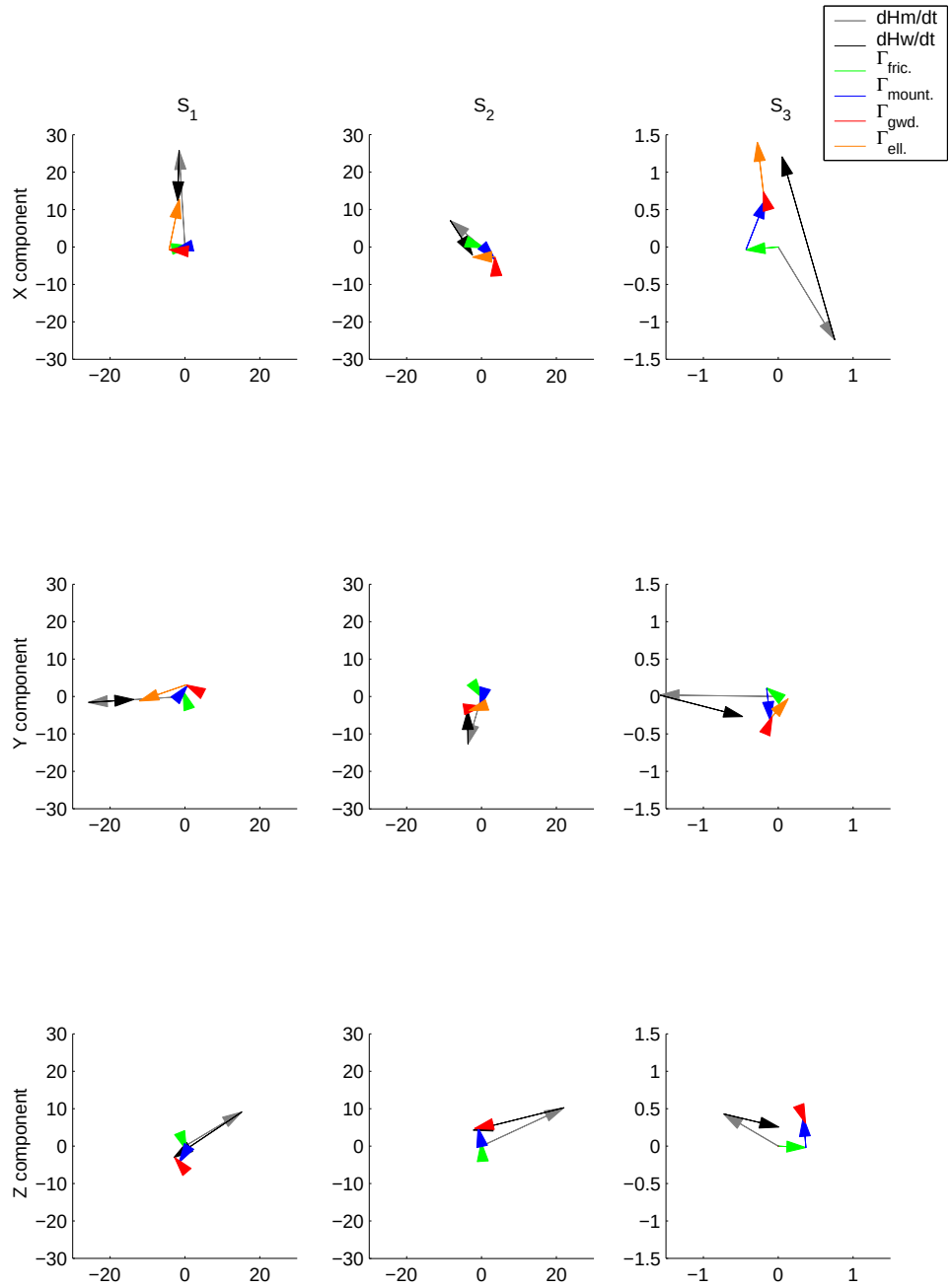

Figure 4. Phase plot of the angular momentum budget, the phase is with respect to 0h00 UT. (unit=Hadleys).

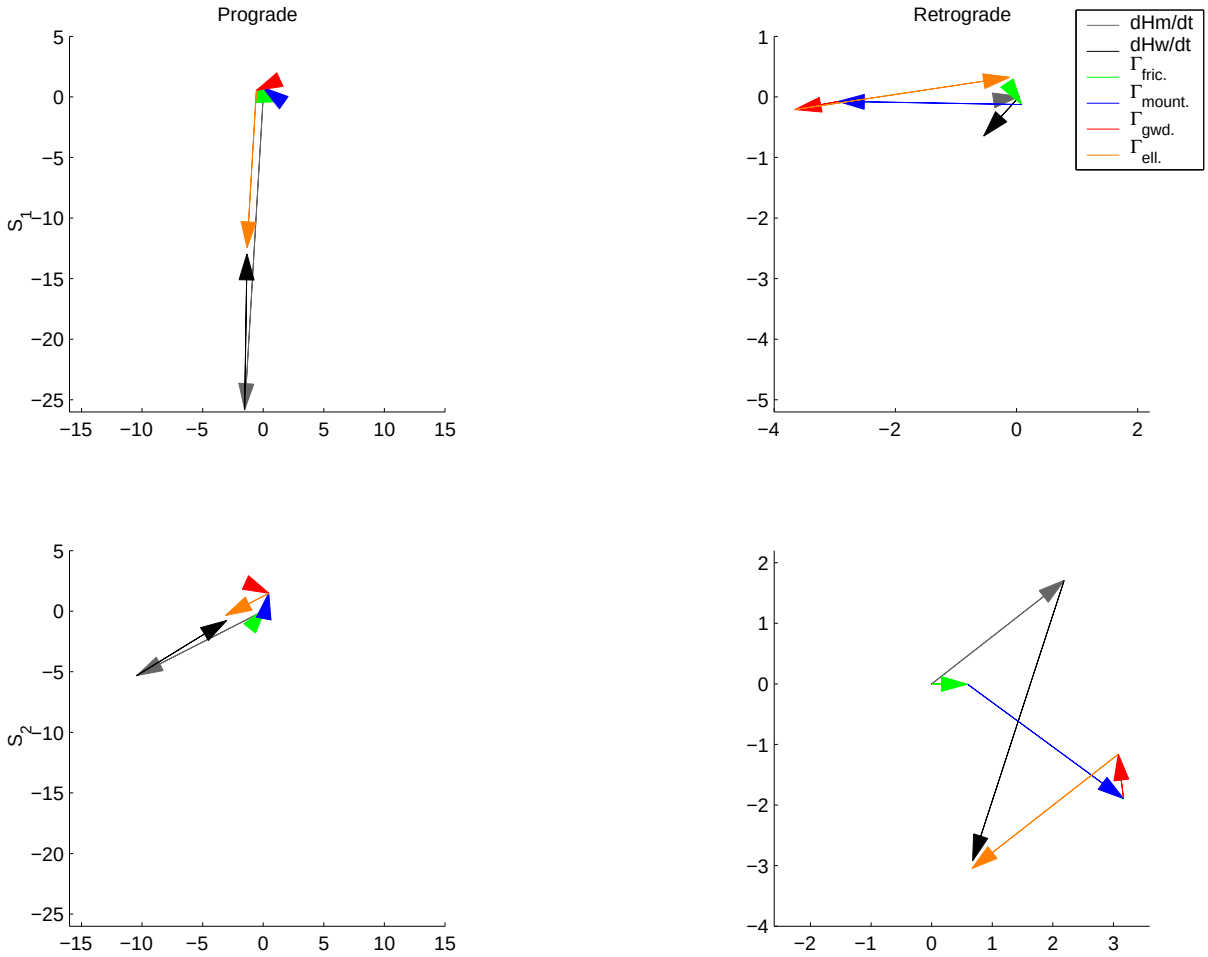

Figure 5. Phase plot of the equatorial angular momentum budget expressed in terms of prograde and retrograde terms, the phase is with respect to 0h00 UT. (unit=Hadleys).

Table 1. Surface pressure spherical harmonics coefficients (in Pa) for the S_1 wave and the three models. The first number is the amplitude of the wave and the second gives the phase. The first line of each model is the real part of the spherical harmonics (in $\cos m\lambda$), while the imaginary part (in $\sin m\lambda$) is given at the second line.

	Model	m =0	1	2	3	4	5	6	7	8	9	10
$\ell = 1$	NCEP	6 *100*°	19 *89*°									
			22 *10*°									
	ECMWF	3 *18*°	19 *132*°									
			22 *51*°									
	LMD	5 *78*°	19 *93*°									
			18 *16*°									
$\ell = 2$	NCEP	12 *-45*°	3 *48*°	8 *76*°								
			5 *49*°	11 *77*°								
	ECMWF	10 *-32*°	2 *72*°	8 *123*°								
			4 *76*°	10 *119*°								
	LMD	12 *-58*°	5 *19*°	10 *88*°								
			5 *78*°	12 *85*°								
$\ell = 3$	NCEP	14 *-108*°	15 *-97*°	4 *166*°	10 *2*°							
			16 *173*°	5 *139*°	8 *118*°							
	ECMWF	12 *-74*°	14 *-63*°	4 *165*°	7 *16*°							
			13 *-145*°	4 *142*°	6 *120*°							
	LMD	12 *-106*°	17 *-83*°	6 *143*°	12 *6*°							
			13 *166*°	6 *145*°	11 *128*°							
$\ell = 4$	NCEP	11 *140*°	5 *-156*°	5 *-106*°	7 *169*°	5 *158*°						
			5 *-110*°	5 *-116*°	9 *165*°	6 *99*°						
	ECMWF	7 *-179*°	2 *-94*°	4 *-77*°	7 *-133*°	4 *-162*°						
			6 *-29*°	4 *-136*°	9 *-155*°	9 *122*°						
	LMD	13 *137*°	5 *-163*°	6 *-102*°	10 *-170*°	1 *63*°						
			4 *-46*°	8 *-150*°	11 *-165*°	15 *106*°						
$\ell = 5$	NCEP	11 *81*°	4 *52*°	3 *-3*°	5 *-136*°	4 *124*°	10 *166*°					
			4 *-64*°	3 *43*°	6 *-129*°	6 *-52*°	12 *85*°					
	ECMWF	13 *129*°	5 *76*°	3 *50*°	5 *-97*°	2 *-144*°	6 *-133*°					
			5 *-54*°	1 *-42*°	6 *-102*°	5 *-3*°	8 *139*°					
	LMD	8 *62*°	11 *102*°	5 *-14*°	4 *-157*°	4 *162*°	12 *-175*°					
			6 *-29*°	2 *-64*°	8 *-123*°	9 *-14*°	13 *121*°					
$\ell = 6$	NCEP	11 *-33*°	4 *-36*°	3 *-14*°	7 *-43*°	4 *135*°	9 *86*°	7 *158*°				
			5 *158*°	5 *-67*°	3 *-40*°	1 *-102*°	11 *-51*°	3 *-28*°				
	ECMWF	8 *28*°	2 *37*°	3 *55*°	7 *-6*°	2 *-168*°	5 *134*°	5 *-133*°				
			6 *-146*°	2 *-6*°	0 *68*°	2 *-6*°	10 *8*°	2 *21*°				
	LMD	10 *-14*°	4 *19*°	7 *15*°	10 *-24*°	4 *-170*°	8 *123*°	10 *-172*°				
			5 *-157*°	4 *1*°	3 *-64*°	7 *-66*°	13 *-13*°	5 *100*°				
$\ell = 7$	NCEP	7 *-128*°	3 *-176*°	5 *-121*°	3 *-34*°	3 *152*°	4 *-22*°	3 *-4*°	5 *165*°			
			1 *72*°	2 *-157*°	4 *66*°	4 *49*°	3 *169*°	4 *-161*°	4 *-53*°			
	ECMWF	9 *-110*°	3 *-154*°	3 *-96*°	3 *22*°	3 *-151*°	5 *71*°	4 *40*°	5 *-130*°			
			4 *139*°	3 *153*°	4 *111*°	2 *101*°	1 *105*°	5 *-153*°	3 *37*°			
	LMD	7 *-150*°	4 *-90*°	1 *137*°	8 *-39*°	5 *-103*°	5 *17*°	4 *26*°	4 *-109*°			
			4 *160*°	2 *122*°	4 *54*°	4 *153*°	6 *-95*°	4 *-157*°	2 *-37*°			
$\ell = 8$	NCEP	11 *-177*°	2 *121*°	5 *131*°	2 *108*°	3 *-79*°	3 *-87*°	3 *5*°	4 *-15*°	3 *-153*°		
			2 *-30*°	6 *85*°	0 *-73*°	3 *47*°	5 *93*°	2 *152*°	2 *-114*°	4 *-71*°		
	ECMWF	7 *-107*°	2 *-172*°	5 *-157*°	3 *144*°	1 *-26*°	2 *-6*°	2 *100*°	4 *57*°	2 *-69*°		
			2 *57*°	3 *165*°	2 *43*°	1 *69*°	3 *177*°	2 *-120*°	1 *-167*°	3 *-9*°		
	LMD	8 *-147*°	3 *-116*°	9 *-171*°	2 *120*°	2 *-76*°	4 *-63*°	4 *12*°	3 *-5*°	5 *-70*°		
			2 *30*°	3 *163*°	5 *59*°	5 *100*°	8 *142*°	5 *-156*°	4 *-134*°	5 *-93*°		
$\ell = 9$	NCEP	7 *-8*°	2 *-18*°	3 *90*°	4 *113*°	2 *70*°	3 *130*°	3 *-57*°	5 *122*°	5 *62*°	5 *83*°	
			3 *-96*°	4 *-98*°	2 *-32*°	2 *107*°	2 *-18*°	1 *125*°	2 *72*°	1 *68*°	1 *-123*°	
	ECMWF	5 *67*°	7 *-27*°	0 *151*°	1 *-156*°	2 *135*°	3 *-138*°	3 *-6*°	3 *-162*°	5 *125*°	1 *121*°	
			2 *-76*°	3 *-47*°	2 *-1*°	1 *148*°	1 *-116*°	0 *-115*°	1 *134*°	3 *130*°	3 *-101*°	
	LMD	3 *33*°	1 *-64*°	3 *-129*°	6 *143*°	5 *98*°	5 *148*°	3 *-17*°	2 *178*°	6 *136*°	1 *-48*°	
			2 *-45*°	3 *-59*°	2 *-142*°	2 *81*°	5 *74*°	3 *88*°	4 *117*°	2 *-173*°	3 *174*°	
$\ell = 10$	NCEP	7 *55*°	2 *-44*°	4 *-22*°	2 *148*°	2 *113*°	1 *-21*°	1 *48*°	3 *104*°	3 *26*°	3 *-33*°	2 *126*°
			1 *-156*°	3 *-87*°	2 *-178*°	2 *-128*°	1 *132*°	2 *-76*°	2 *60*°	3 *-26*°	3 *104*°	1 *14*°
	ECMWF	7 *92*°	1 *-145*°	4 *3*°	3 *-130*°	1 *137*°	2 *-102*°	1 *13*°	3 *177*°	2 *26*°	2 *46*°	1 *-154*°
			3 *-39*°	3 *-33*°	1 *-4*°	1 *46*°	2 *-177*°	1 *-122*°	2 *107*°	2 *32*°	2 *176*°	2 *-107*°
	LMD	4 *100*°	2 *-1*°	6 *-9*°	3 *-142*°	3 *84*°	3 *81*°	2 *87*°	2 *130*°	3 *65*°	3 *100*°	2 *-78*°
			3 *-115*°	1 *-72*°	4 *-139*°	1 *-139*°	2 *-84*°	6 *-2*°	4 *62*°	2 *-4*°	4 *140*°	1 *-164*°

Table 2. Surface pressure spherical harmonics coefficients (in Pa) for the S_2 wave and the three models. The first number is the amplitude of the wave and the second gives the phase. As there is only 4 points a day in the NCEP model, it is impossible to give an estimation of the phase, and the estimation of the amplitude is to be considered with caution. The first line of each model is the real part of the spherical harmonics (in $\cos m\lambda$), while the imaginary part (in $\sin m\lambda$) is given at the second line.

	Model	m =0	1	2	3	4	5	6	7	8	9	10
$\ell = 1$	NCEP	1 ×	3 ×									
			2 ×									
	ECMWF	3 *-128°*	3 *126°*									
			2 *87°*									
	LMD	0 *26°*	2 *101°*									
			2 *15°*									
$\ell = 2$	NCEP	11 ×	3 ×	40 ×								
			6 ×	51 ×								
	ECMWF	23 *52°*	2 *98°*	67 *24°*								
			4 *-139°*	64 *-67°*								
	LMD	9 *-65°*	2 *17°*	58 *-43°*								
			2 *-179°*	56 *-134°*								
$\ell = 3$	NCEP	4 ×	3 ×	7 ×	1 ×							
			0 ×	3 ×	7 ×							
	ECMWF	7 *55°*	2 *-81°*	3 *22°*	5 *42°*							
			1 *-130°*	3 *47°*	5 *50°*							
	LMD	3 *14°*	2 *-36°*	4 *-5°*	5 *-88°*							
			1 *119°*	2 *-65°*	7 *-46°*							
$\ell = 4$	NCEP	9 ×	2 ×	13 ×	1 ×	0 ×						
			2 ×	14 ×	2 ×	1 ×						
	ECMWF	11 *-131°*	1 *-167°*	14 *-159°*	2 *45°*	3 *-78°*						
			2 *46°*	14 *115°*	1 *-116°*	2 *45°*						
	LMD	5 *81°*	1 *-175°*	18 *136°*	2 *56°*	3 *-53°*						
			1 *11°*	18 *49°*	1 *-135°*	5 *51°*						
$\ell = 5$	NCEP	4 ×	2 ×	3 ×	2 ×	0 ×	3 ×					
			1 ×	1 ×	1 ×	1 ×	1 ×					
	ECMWF	3 *-61°*	2 *50°*	1 *-128°*	1 *129°*	3 *101°*	2 *70°*					
			2 *-111°*	3 *-103°*	2 *-128°*	2 *109°*	1 *14°*					
	LMD	0 *-117°*	1 *157°*	1 *45°*	3 *69°*	1 *92°*	2 *14°*					
			1 *-140°*	2 *-102°*	1 *110°*	1 *34°*	1 *-14°*					
$\ell = 6$	NCEP	4 ×	0 ×	0 ×	1 ×	1 ×	0 ×	2 ×				
			3 ×	2 ×	3 ×	1 ×	2 ×	1 ×				
	ECMWF	3 *34°*	2 *26°*	2 *-74°*	2 *-103°*	1 *-115°*	2 *-5°*	4 *102°*				
			0 *-118°*	0 *60°*	1 *152°*	1 *72°*	0 *-69°*	2 *7°*				
	LMD	0 *-108°*	1 *102°*	2 *-47°*	1 *-163°*	1 *156°*	1 *-48°*	2 *59°*				
			1 *112°*	3 *-111°*	1 *-131°*	0 *95°*	0 *-126°*	1 *-77°*				
$\ell = 7$	NCEP	6 ×	2 ×	3 ×	2 ×	1 ×	0 ×	2 ×	0 ×			
			0 ×	0 ×	1 ×	0 ×	3 ×	2 ×	0 ×			
	ECMWF	4 *162°*	1 *-95°*	1 *49°*	2 *-73°*	2 *-113°*	1 *-3°*	2 *-24°*	1 *105°*			
			2 *100°*	0 *23°*	1 *34°*	2 *6°*	1 *-134°*	2 *-105°*	2 *-50°*			
	LMD	0 *28°*	1 *107°*	1 *-108°*	2 *-116°*	1 *-145°*	0 *-74°*	2 *-36°*	2 *50°*			
			1 *79°*	1 *107°*	0 *-135°*	1 *66°*	1 *-10°*	1 *-120°*	1 *-87°*			
$\ell = 8$	NCEP	0 ×	0 ×	2 ×	3 ×	0 ×	0 ×	1 ×	1 ×	1 ×		
			1 ×	2 ×	1 ×	1 ×	1 ×	2 ×	1 ×	1 ×		
	ECMWF	5 *59°*	0 *-147°*	2 *104°*	1 *-32°*	2 *99°*	1 *134°*	1 *-112°*	1 *-107°*	1 *135°*		
			2 *54°*	1 *38°*	2 *2°*	1 *-46°*	2 *54°*	1 *141°*	1 *-174°*	1 *-56°*		
	LMD	1 *-99°*	1 *88°*	1 *6°*	1 *-20°*	0 *-138°*	0 *86°*	1 *-157°*	0 *-132°*	1 *81°*		
			1 *-73°*	0 *24°*	0 *1°*	1 *53°*	1 *10°*	0 *118°*	1 *120°*	1 *-130°*		
$\ell = 9$	NCEP	6 ×	3 ×	1 ×	5 ×	1 ×	0 ×	1 ×	0 ×	0 ×	0 ×	
			0 ×	0 ×	0 ×	0 ×	0 ×	0 ×	2 ×	0 ×	1 ×	
	ECMWF	1 *128°*	1 *143°*	1 *90°*	1 *55°*	1 *91°*	1 *93°*	2 *36°*	1 *-28°*	2 *-35°*	1 *-109°*	
			0 *-152°*	0 *-119°*	1 *29°*	1 *-93°*	2 *112°*	1 *-140°*	1 *-178°*	0 *-160°*	2 *151°*	
	LMD	1 *-148°*	0 *-106°*	1 *129°*	1 *56°*	1 *10°*	1 *44°*	1 *149°*	1 *-174°*	0 *-149°*	1 *-136°*	
			1 *-84°*	1 *79°*	1 *11°*	0 *1°*	1 *-96°*	1 *25°*	1 *122°*	1 *105°*	1 *93°*	
$\ell = 10$	NCEP	3 ×	0 ×	0 ×	1 ×	0 ×	2 ×	0 ×	0 ×	1 ×	0 ×	0 ×
			4 ×	1 ×	1 ×	1 ×	1 ×	0 ×	1 ×	1 ×	2 ×	0 ×
	ECMWF	4 *-108°*	1 *33°*	1 *-15°*	1 *-121°*	1 *-163°*	1 *60°*	0 *-138°*	1 *-155°*	0 *23°*	1 *37°*	1 *143°*
			2 *75°*	1 *-109°*	1 *-92°*	1 *-119°*	1 *-67°*	1 *-71°*	0 *89°*	0 *59°*	1 *-93°*	2 *119°*
	LMD	1 *102°*	1 *-84°*	1 *-143°*	1 *149°*	1 *88°*	1 *20°*	1 *35°*	0 *-151°*	0 *6°*	0 *28°*	1 *127°*
			0 *60°*	1 *-165°*	1 *50°*	0 *33°*	1 *-125°*	2 *-91°*	0 *146°*	1 *15°*	1 *-24°*	1 *92°*

Table 3. Surface pressure spherical harmonics coefficients (in Pa) for the S_3 wave and the three models. The first number is the amplitude of the wave and the second gives the phase. As there is only 4 points a day in the NCEP model, it is impossible to give an estimation of the phase, and the estimation of the amplitude is to be considered with caution. The first line of each model is the real part of the spherical harmonics (in $\cos m\lambda$), while the imaginary part (in $\sin m\lambda$) is given at the second line.

	Model	m =0	1	2	3	4	5	6	7	8	9	10
$\ell = 1$	ECMWF	0 *-114*°	1 *-90*°									
			0 *162*°									
	LMD	0 *-80*°	0 *-108*°									
			0 *108*°									
$\ell = 2$	ECMWF	2 *98*°	0 *96*°	1 *-71*°								
			0 *-66*°	1 *-115*°								
	LMD	0 *59*°	0 *-132*°	0 *-95*°								
			0 *96*°	0 *-119*°								
$\ell = 3$	ECMWF	0 *148*°	1 *-119*°	1 *32*°	3 *-178*°							
			4 *-74*°	1 *-97*°	1 *58*°							
	LMD	0 *-85*°	0 *75*°	0 *-91*°	1 *-4*°							
			1 *63*°	0 *-162*°	1 *-76*°							
$\ell = 4$	ECMWF	1 *147*°	1 *93*°	1 *116*°	2 *165*°	1 *-75*°						
			1 *164*°	1 *55*°	1 *178*°	1 *-133*°						
	LMD	1 *14*°	0 *-57*°	1 *-136*°	3 *80*°	2 *161*°						
			1 *95*°	2 *-72*°	4 *139*°	1 *117*°						
$\ell = 5$	ECMWF	1 *-61*°	1 *29*°	1 *-69*°	2 *-161*°	1 *31*°	2 *176*°					
			1 *160*°	0 *22*°	3 *138*°	1 *-103*°	2 *75*°					
	LMD	1 *40*°	0 *102*°	0 *-142*°	1 *-154*°	1 *-137*°	1 *-102*°					
			1 *91*°	0 *152*°	0 *-138*°	0 *-42*°	0 *-90*°					
$\ell = 6$	ECMWF	0 *-84*°	1 *-135*°	0 *-92*°	1 *-21*°	0 *-9*°	1 *66*°	1 *-150*°				
			1 *82*°	0 *-23*°	2 *-84*°	1 *-41*°	1 *-64*°	0 *122*°				
	LMD	1 *-169*°	0 *69*°	0 *35*°	1 *-109*°	1 *-88*°	1 *-92*°	1 *-130*°				
			0 *163*°	1 *83*°	0 *3*°	1 *-127*°	0 *-125*°	0 *63*°				
$\ell = 7$	ECMWF	0 *123*°	1 *-138*°	1 *165*°	0 *-140*°	0 *162*°	3 *-7*°	1 *111*°	1 *-25*°			
			0 *169*°	0 *74*°	1 *-37*°	1 *101*°	2 *72*°	1 *-160*°	2 *-42*°			
	LMD	0 *-138*°	0 *-149*°	0 *2*°	0 *43*°	0 *6*°	0 *16*°	0 *123*°	1 *-134*°			
			1 *-128*°	0 *-75*°	1 *24*°	0 *-108*°	0 *-117*°	0 *28*°	1 *66*°			
$\ell = 8$	ECMWF	1 *117*°	0 *58*°	1 *97*°	1 *71*°	1 *126*°	1 *87*°	0 *39*°	0 *-179*°	1 *-81*°		
			0 *173*°	0 *-175*°	1 *112*°	1 *117*°	0 *133*°	0 *-175*°	0 *-134*°	0 *-110*°		
	LMD	1 *-1*°	0 *-161*°	0 *-143*°	0 *134*°	1 *70*°	0 *17*°	1 *21*°	0 *114*°	1 *-141*°		
			0 *-76*°	0 *-120*°	0 *-111*°	1 *-2*°	0 *-107*°	0 *-162*°	1 *43*°	0 *101*°		
$\ell = 9$	ECMWF	0 *-141*°	2 *111*°	0 *-70*°	1 *109*°	0 *114*°	0 *109*°	0 *112*°	0 *101*°	0 *26*°	1 *-84*°	
			0 *-79*°	1 *-68*°	0 *-96*°	1 *-91*°	1 *113*°	0 *130*°	0 *71*°	0 *65*°	0 *-126*°	
	LMD	0 *56*°	0 *-14*°	0 *-130*°	0 *-110*°	0 *45*°	0 *154*°	0 *-37*°	0 *34*°	0 *83*°	0 *-152*°	
			0 *-3*°	0 *105*°	0 *178*°	0 *-15*°	0 *-23*°	0 *-146*°	1 *-126*°	0 *-162*°	0 *-49*°	
$\ell = 10$	ECMWF	1 *-93*°	0 *-81*°	1 *89*°	0 *-6*°	0 *82*°	0 *-135*°	0 *-101*°	1 *98*°	0 *105*°	0 *151*°	0 *-56*°
			1 *131*°	0 *110*°	0 *-53*°	0 *-110*°	0 *118*°	0 *15*°	0 *115*°	0 *72*°	0 *86*°	0 *111*°
	LMD	0 *-159*°	0 *10*°	0 *15*°	0 *-22*°	0 *-125*°	0 *153*°	1 *175*°	0 *-87*°	0 *8*°	0 *59*°	0 *110*°
			0 *4*°	0 *51*°	0 *72*°	0 *159*°	0 *26*°	0 *58*°	0 *-83*°	0 *-132*°	0 *-176*°	0 *-102*°

Table 4. Diurnal and sub-diurnal effect on the Earth rotation. The amplitude of the polar motion is given in μas and of the LOD variation in μs. The phase (in italic) is given in hour with respect to 0h00 UT.

	Polar motion X			Polar motion Y			LOD variations		
	LMD	ECMWF	NCEP	LMD	ECMWF	NCEP	LMD	ECMWF	NCEP
S_1	188,*-2.69*	390,*-1.85*	121,*-2.369*	231,*-1.83*	1084,*-1.81*	196,*-2.31*	2,*9.45*	29,*-3.86*	5, *-6.00*
S_2	1,*3.12*	13,*1.32*	3.82	1,*1.76*	10,*-2.01*	2	1,*-11.14*	35,*-9.64*	1, *X*
S_3	0.1,*0.16*	1,*1.94*		0	0.3,*0.35*		0	9,*5.07*	

Table 5. Diurnal and sub-diurnal effect on the geocenter in mm. The phase (in italic) is given in hour with respect to 0h00 UT.

	X			Y			Z		
	LMD	ECMWF	NCEP	LMD	ECMWF	NCEP	LMD	ECMWF	NCEP
S_1	0.70,-*0.24*	0.69,-*2.84*	0.70,*0.01*	0.65,*4.9*	0.82,*2.58*	0.83,*5.27*	0.09,*0.792*	0.05,*4.68*	0.11,-*0.71*
S_2	0.06,-*0.80*	0.11,-*2.40*		0.07,*4.95*	0.08,*0.162*		0	0.05,-*9.45*	
S_3	0	0.04,-*11.94*		0	0.01,-*4.83*		0	0	